Image Hiding Based on Circular Moiré Fringes

MINVYDAS RAGULSKIS
Department of Mathematical Research in Systems
Kaunas University of Technology
Studentu 50, Kaunas LT-51368
LITHUANIA
minvydas.ragulskis@ktu.lt http://www.personalas.ktu.lt/~mragul

ALGIMENT ALEKSA
Department of Mathematical Research in Systems
Kaunas University of Technology
Studentu 50, Kaunas LT-51368
LITHUANIA
algiment.aleksa@ktu.lt http://www.personalas.ktu.lt/~mragul

JURATE RAGULSKIENE
Department of Technical Sciences
Kauno Kolegija
Pramones 20, Kaunas LT-50468
LITHUANIA
jurate352@gmail.com http://www.kauko.lt

Abstract: - Circular time-averaging moiré technique is exploited to hide an image in a background moiré grating. The secret image can be visualized when the encoded image is oscillated around a pre-defined axial point. It is a new visual decoding scheme when the secret image is embedded into a circular moiré grating and can be interpreted by a naked eye. The encoded secret image is not shared into components; this is a one image method. Computational examples are used to demonstrate the functionality of the method. The property of the human visual system to average fast dynamical processes being not able to follow rapid oscillatory motions is exploited to decode the secret image.

Key-Words: - Visual Cryptography, Moiré fringes, Bessel Functions

1 Introduction

Visual cryptography is a cryptographic technique which allows visual information (pictures, text, etc.) to be encrypted in such a way that the decryption can be performed by the human visual system, without the aid of computers. Visual cryptography was pioneered by Naor and Shamir in 1994 [1]. They demonstrated a visual secret sharing scheme, where an image was broken up into n shares so that only someone with all n shares could decrypt the image, while any $n-1$ shares revealed no information about the original image. Each share was printed on a separate transparency, and decryption was performed by overlaying the shares. When all n shares were overlaid, the original image would appear. Since 1994, many advances in visual cryptography have been done; few references [2 – 9] can illustrate the dynamism of the field.

Geometric moiré [10, 11] is a classical in-plane whole-field non-destructive optical experimental technique based on analysis of visual patterns produced by superposition of two regular gratings that geometrically interfere. Two basic goals exist in moiré pattern research. The first is the analysis of moiré patterns. The task is to analyze and characterize the distribution of moiré fringes in a moiré pattern. Most of the research in moiré pattern analysis deals with the interpretation of experimentally produced patterns of fringes and determination of displacements (or strains) at centerlines of appropriate moiré fringes [12].

Another goal is moiré pattern synthesis when the generation of a certain predefined moiré pattern is required [13, 14]. The synthesis process involves production of such two images that the required moiré pattern emerges when those images are superimposed. Moiré synthesis and analysis are tightly linked and understanding one task gives insight into the other.

Image hiding method based on time-averaging moiré is proposed in [15]. This method is based not on static superposition of moiré images, but on time-averaging geometric moiré. This method generates only one picture; the secret image can be interpreted by a naked eye only when the original encoded image is harmonically oscillated in a predefined direction at strictly defined amplitude of oscillation. This method resembles a visual cryptography scheme because one needs a computer to encode a secret, but one can decode the secret without a computing device. Only one picture is generated, and the secret is leaked from this picture when parameters of the oscillation are appropriately tuned. In other words, the secret can be decoded by trial and error (if only one knows that he has to shake the slide). Therefore, additional image security measures are implemented in [15], particularly splitting of the encoded image into two shares. Oscillation of any of the shares separately does not reveal the secret. Two shares must be superimposed and then oscillated before the secret image can be interpreted.

The security of the image encoding is even more increased in [16]. A special image encoding method is developed which reveals the secret image not only at exactly tuned parameters of the oscillation, but also requires that the time function determining the process of oscillation would comply with specific requirements. Moreover, this method does not reveal the secret image at any amplitude of harmonic oscillations. Instead, the secret should be leaked only at carefully chosen parameters of this specific time function.

The object of this paper is to develop a new scheme for visualization of secret images. A secret image can be interpreted by a naked eye only when the original encoded image is harmonically oscillated in angular direction around a predefined internal point of the image. This visual decoding technique requires only one image. Moreover, the secret image is visualized only at strictly defined amplitude of oscillation.

This paper is organized as follows. The formation of time-averaged moiré fringes is discussed in Section 2; encoding of a secret image into a circular moiré grating is presented in Section 3; the principles of visual decoding of the secret image are discussed in Section 4 and concluding remarks are given in the final Section.

2 Optical Background

Moiré grating on the surface of a one-dimensional structure in the state of equilibrium can be interpreted as a periodic variation of black and white colors [17]:

$$M(y)=\frac{1}{2}+\frac{1}{2}\cos\left(\frac{2\pi}{\lambda}y\right), \tag{1}$$

where y is the longitudinal coordinate; $M(y)$ is grayscale level of the surface at point y; λ is the pitch of the grating. Numerical value 0 of the function in (eq. (1)) corresponds to black; 1 – to white; all intermediate values – to appropriate grayscale levels.

If the deflection from the state of equilibrium is u, then the moiré grating becomes $M(y-u)$. But if these deflections oscillate in time:

$$u(x,t)=a(x)\sin(\omega t+\phi), \tag{2}$$

where a is the amplitude of harmonic oscillations; ω is the circular frequency; ϕ is the phase; time averaged moiré grating can be described by [18]:

$$\begin{aligned}
&M_T(x,y)=\\
&\lim_{T\to\infty}\frac{1}{T}\int_0^T\left(\frac{1}{2}+\frac{1}{2}\cos\left(\frac{2\pi}{\lambda}\left(y-a(x)\sin(\omega t+\phi)\right)\right)\right)dt=\\
&\frac{1}{2}+\frac{1}{2}\cos\left(\frac{2\pi}{\lambda}y\right)\lim_{T\to\infty}\frac{1}{T}\int_0^T\cos\left(\frac{2\pi}{\lambda}a(x)\sin t\right)dt\\
&+\frac{1}{2}\sin\left(\frac{2\pi}{\lambda}y\right)\lim_{T\to\infty}\frac{1}{T}\int_0^T\sin\left(\frac{2\pi}{\lambda}a(x)\sin t\right)dt.
\end{aligned} \tag{3}$$

where T is the exposure time. But

$$\begin{aligned}
&\lim_{T\to\infty}\frac{1}{T}\int_0^T\sin\left(\frac{2\pi}{\lambda}a(x)\sin t\right)dt=\\
&\frac{1}{\pi}\int_{-\frac{\pi}{2}}^{\frac{\pi}{2}}\sin\left(\frac{2\pi}{\lambda}a(x)\sin t\right)dt=0
\end{aligned} \tag{4}$$

due to the oddness of the sine function. Therefore, adding an imaginary term reduces Eq. (3) to the following form:

$$M_T(x,y)=\frac{1}{2}+\frac{1}{2}\cos\left(\frac{2\pi}{\lambda}y\right)\cdot\left(\lim_{T\to\infty}\frac{1}{T}\int_0^T\left(\begin{array}{l}\cos\left(\frac{2\pi}{\lambda}a(x)\sin t\right)\\+i\sin\left(\frac{2\pi}{\lambda}a(x)\sin t\right)\end{array}\right)dt\right)=\frac{1}{2}+\frac{1}{2}\cos\left(\frac{2\pi}{\lambda}y\right)J_0\left(\frac{2\pi}{\lambda}a(x)\right) \qquad (5)$$

where i is the imaginary unit; J_0 is the zero order Bessel function of the first kind:

$$J_0(x)=\lim_{T\to\infty}\frac{1}{T}\int_0^T\exp(ix\sin t)dt\,. \qquad (6)$$

Time averaged fringes will form at such x where $J_0\left(\frac{2\pi}{\lambda}a(x)\right)=0$. Now the relationship between the fringe order, the amplitude of oscillations and the pitch of the grating takes the following form:

$$\frac{2\pi}{\lambda}a_i(x)=r_i\,, \qquad (7)$$

where r_i denotes i-th root of the zero order Bessel function of the first kind; a_i is the amplitude of oscillation at the center of the i-th fringe; and the fringe order is determined using automatic, semiautomatic or even manual fringe counting techniques applied to the experimental pattern of fringes.

The envelope function modulating the harmonic moiré grating is then expressed in the following form:

$$E(a)=\frac{1}{2}\pm\frac{1}{2}J_0\left(\frac{2\pi}{\lambda}a\right). \qquad (8)$$

Computational reconstruction of time-averaged fringes can be implemented directly computing the limit sum:

$$M_T(x,y)=\frac{1}{2}+\frac{1}{2}\cos\left(\frac{2\pi}{\lambda}y\right)\cdot\lim_{n\to\infty}\frac{1}{n}\sum_{k=0}^{n-1}\cos\left(\frac{2\pi}{\lambda}a(x)\sin\left(\frac{2\pi k}{n}\right)\right), \qquad (9)$$

where $n\in N$. A regular moiré grating in the state of equilibrium is shown in Fig. 1A; a statically deformed grating is illustrated in Fig. 1B ($a=0.1x$); double exposure (arithmetic average) produced the well-known effect of beatings (Fig. 1C); time averaged image shows fringes, but the overall image looses contrast at increasing amplitudes of oscillation (Fig. 1D).

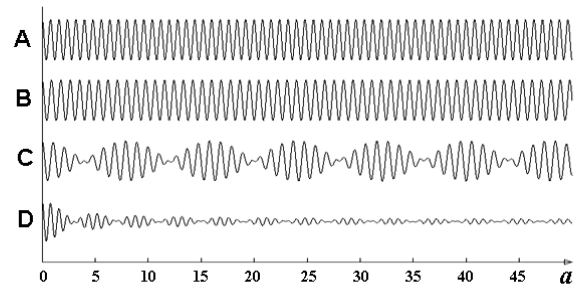

Fig. 1. Computational illustration of time-averaged moiré fringes: A – moiré grating in the state of equilibrium; B – deformed grating; C – double exposure of A and B; D – time-averaged fringes.

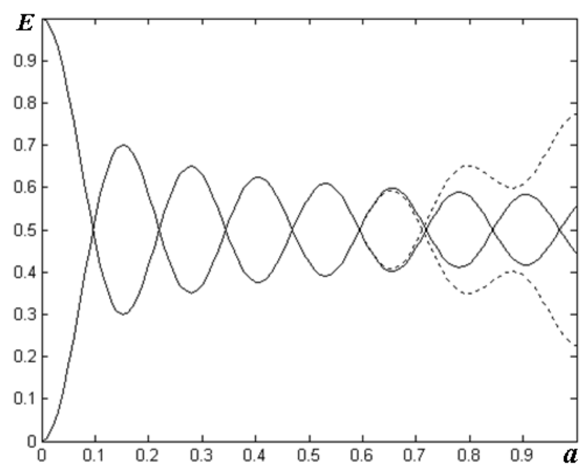

Fig. 2. Illustration of the time-averaged envelope function; solid lines denote analytical solution; dotted lines denote approximate computational solution at n = 30.

The modulating envelope function (Eq. (8)) is illustrated in Fig. 2. Intersections between solid lines represent roots of the zero order Bessel function of the first kind.

Computationally reconstructed pattern of time averaged fringes is presented in Fig. 3. Static moiré grating is formed in the interval $0\le y\le 5$ ($\lambda=0.2$); white background is assumed elsewhere.

It is assumed that $a(x) = x$. Therefore clear moiré grating is visible at the left part of the time averaged image which gets blurred as the amplitude of harmonic oscillations increases. As mentioned previously, the decline of contrast of the time averaged image is modulated by the zero order Bessel function of the first kind (Eq. (8)). It can be noted that the frequency of oscillations has no effect to the formation of fringes (Eq. (5)). Exposure time must be long enough to fit in a large number of periods of oscillations (or alternatively must be exactly equal to one period of oscillation).

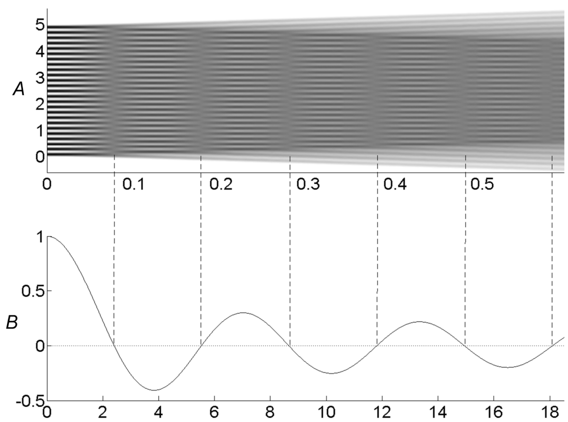

Fig. 3. Pattern of time averaged fringes at $\lambda = 0.2$; $a(x) = x$; A – grayscale time averaged image; B – zero order Bessel function of the first kind; dashed lines are used to interconnect the centers of time averaged fringes and roots of the Bessel function.

3 Encoding an Image into a Circular Moiré Grating

Circular moiré grating is constructed as a set of concentric circles around internal image point (x_0, y_0). It is not necessary that the center of moiré grating would be a central point in the encoded image. Each concentric circle is created as a set of grayscale pixel's formed according to Eq. (1) where the longitudinal coordinate y is replaced by the angular coordinate φ (unidirectional oscillations along the y-axis are replaced by angular oscillations around the central point).

Digital time averaged image is now computed as an integral sum in the circular direction analogously to Eq. (9). The assumption that the amplitude of harmonic angular oscillations a is constant in the area of the whole image yields:

$$M_T(x, y) = \lim_{n\to\infty} \frac{1}{n} \sum_{k=0}^{n-1} \frac{1}{2}\left(1 + \cos\left(\frac{2\pi}{\lambda}\left(\varphi_0 + a \sin\left(\frac{2\pi k}{n}\right)\right)\right)\right) \quad (10)$$

where n is the number of discrete nodes in a period of harmonic angular oscillations, and φ_0 is the angular coordinate of the current point (x, y) in respect to the central point of angular oscillations:

$$\varphi_0 = \begin{cases} \arctan\left(\frac{y_0 - y}{x - x_0}\right), & if\ (x > x_0)\ \&\ (y <= y_0), \\ \pi - \arctan\left(\frac{y_0 - y}{x - x_0}\right), & if\ (x < x_0) \& (y <= y_0), \\ \pi + \arctan\left(\frac{y - y_0}{x_0 - x}\right), & if\ (x < x_0)\ \&\ (y >= y_0), \\ 2\pi - \arctan\left(\frac{y - y_0}{x - x_0}\right), & if\ (x > x_0)\ \&\ (y >= y_0), \\ \frac{\pi}{2}, & if\ (x = x_0)\ \&\ (y < y_0), \\ \frac{3\pi}{2}, & if\ (x = x_0)\ \&\ (y > y_0), \\ 0, & if\ (x = x_0)\ \&\ (y = y\ ) \end{cases} \quad (11)$$

The process of computation reconstruction of time-averaged circular fringes is illustrated in Fig. 4 where additive superposition is used to calculate the time average of an arc of a single moiré circle.

The formation of time-averaged fringes is illustrated in Fig. 5. Two circular moiré gratings are formed in the upper and the lower parts if the image in Fig. 5A. Initially we select such amplitude of angular oscillations that the time-average fringe would form in the top part of the image (the amplitude is determined from Eq. (7) using the first root of the Bessel function of the first kind). Then the same procedure is repeated for the bottom part of the image (Figs. 5B and 5C). Finally, the process is repeated at such an amplitude when no time-averaged fringes are formed (Fig. 5D).

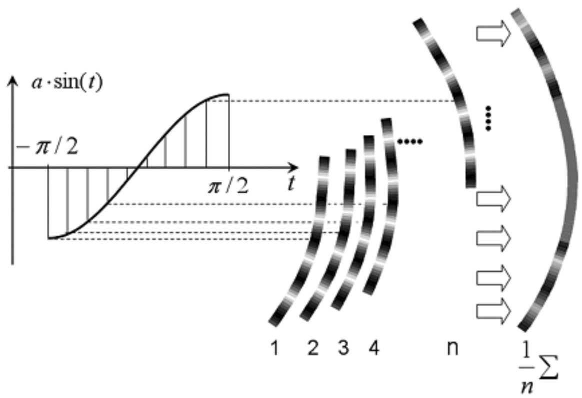

Fig. 4. A schematic diagram illustrating the computational reconstruction of a time-averaged image.

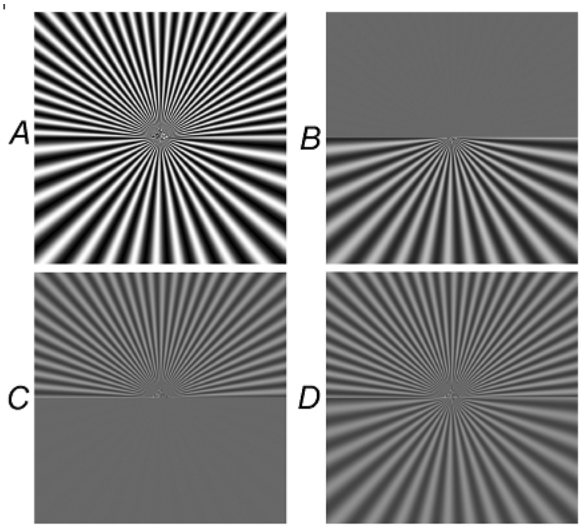

Fig. 5. Illustration of the formation time-averaged fringes: A – static image, the pitch of the moiré grating at the upper half of the image is 0.1; the pitch at the lower half is 0.18; B – time-averaged image at a = 0.0383; C – time-averaged image at a = 0.0689; D – an incorrect amplitude does not produce time averaged fringes.

Though the angular pitch of the circular moiré grating is fixed, the physical distance between grating lines depends on the distance from the center point. That limits the ability to encode larger amount of digital information. Therefore we split the circular moiré grating into several bands (Fig. 6). For each band we select different pitches used for the secret image (compare to Eq. (7)):

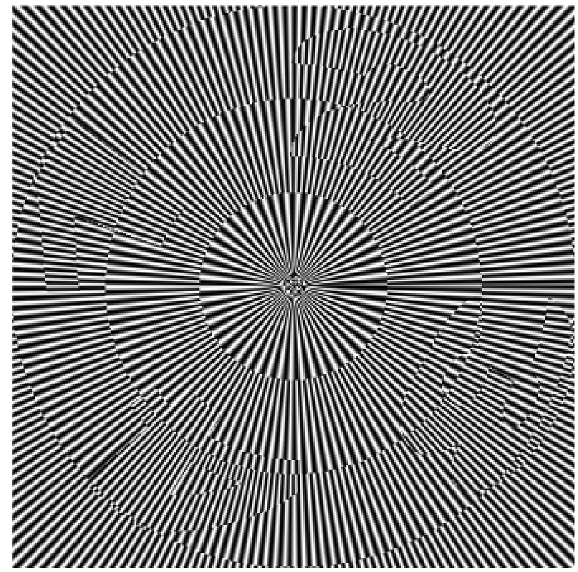

Fig. 6. Encryption of the secret text “1234” into the moiré grating comprised from four circular bands. Pitches of the secret image and the background in first band are: $\lambda_1 = 0.1$; $\lambda_{1b} = 0.1266$; in the second band: $\lambda_2 = 0.0436$; $\lambda_{2b} = 0.0552$; in the third band: $\lambda_3 = 0.0278$; $\lambda_{3b} = 0.0352$; and in the fourth band: $\lambda_4 = 0.0204$; $\lambda_{4b} = 0.0258$.

$$\lambda_i = \frac{2\pi a}{r_i};\ i = 1,2,\ldots. \qquad (12)$$

Thus we ensure that time-averaged fringes will form in all bands (at appropriate locations), though we exploit different roots of the zero order Bessel function of the first kind in different bands.

Moreover, we use the stochastic phase deflection algorithm [15] to increase the security of the encryption (this algorithm is of course adapted to the circular moiré grating). A schematic illustration of this algorithm is shown in Fig. 9; the encrypted image – in Fig. 10. The phases of adjacent moiré circles at the right section of Fig. 9 are selected in random, while locations of the secret image (gray zones) are not altered.

Since the digital image is constructed as a set of concentric circles, every single circle corresponds to a set of grayscale pixels. Variation of the grayscale level in the zone of the background image corresponds to the pitch λ_0. Variation of the grayscale level in the areas occupied by the encrypted text must correspond to one of the pitches calculated from Eq. (12).

Moreover, we select appropriate phases of the harmonic variation of the grayscale levels in different zones of the digital image in order to avoid discontinuities (Fig. 7). We illustrate the necessity of this phase matching using both a line graph and a grayscale level map. The zone of the encrypted text is shaded for clarity. One circle of pixels (before and after the matching of phases) is shown. Circles are placed horizontally in order to minimize the size of the figure.

Simple embedding of text “1234” in a background moiré image would produce an unsatisfactory result (Fig. 6) – the “secret” information can be easily recognized by a naked eye. Therefore we use stochastic phase deflection of adjacent circles of pixels. This procedure is illustrated in Fig. 8 where two adjacent circles of pixels are presented after the initial random phase at the left side of the image is already assigned. Gray shaded zones in Fig. 8 are plotted different as we operate with two different circles of pixels. Phases are matched at boundaries of the background and the encoded image.

Such random scrambling of initial phases may appear similar to the concept of stochastic geometric moiré presented in [19]. In fact, these two concepts are completely different – pixels of the background image are not shifted from their original locations in contrary to the technique exploited in [19].

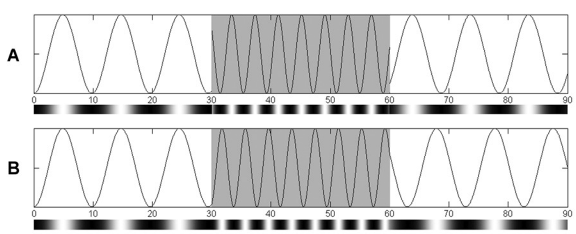

Fig. 7. Matching of phases at boundaries of the background image and the encrypted image; variations of grayscale levels before the matching (A) and after the matching (B) are shown.

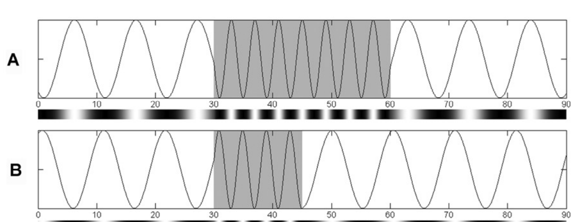

Fig. 8. Illustration of the procedure of stochastic deflection of phases for adjacent columns of pixels.

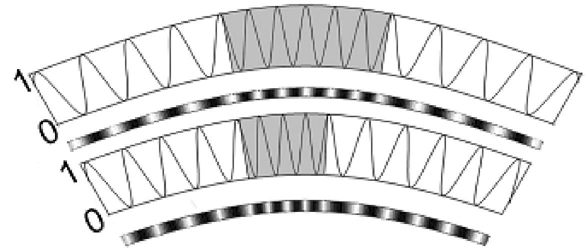

Fig. 9. A schematic illustration of the stochastic phase deflection algorithm applied to adjacent concentric moiré circles; white areas represent the background; gray zones stand for the secret image.

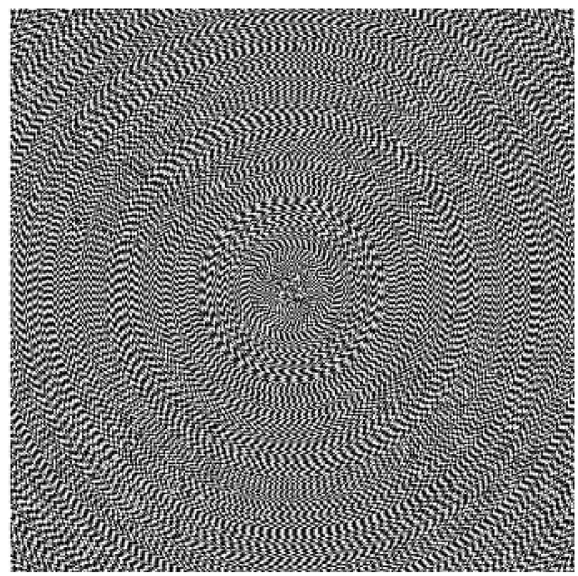

Fig. 10. The encrypted image; the stochastic phase deflection algorithm is applied to the circular moiré grating.

4 Visual Decoding of the Secret Image

The functionality of the decoding procedure is demonstrated in Fig. 11. The embedded secret text “1234” is visible as a pattern of gray time-averaged fringes (the amplitude of angular oscillations is pre-selected according to Eq. (12)), but the moiré grating in the background is not transformed into a gray zone. Alternatively, the background can be transformed into a gray zone at an appropriate amplitude (then the secret image would stay rippled), but we omit the illustration for the brevity. But visualization of the secret text is not possible if either the zones corresponding to the secret text or the background are not transformed into a pattern of gray time-averaged fringes (Fig. 13).

Our proposed method could be considered to be somewhat similar to the moiré cryptography method proposed by Desmedt and Van Lee [13]. But there is a principal difference between optical techniques used in [13] and in our approach. Double exposure geometric moiré (a superposition of two moiré slides) is used in [13]. We use time-averaging geometric moiré optical technique. There are no 2 or n shares to superpose in our method. We use one image only. We oscillate that image in order to produce time-averaged moiré fringes. This is in contrary to interference between two static moiré gratings. The formation of time-averaged fringes is governed by different physical processes compared to double exposure fringes; motion induced blur is exploited to generate time-averaged fringes. Thus, the similarity between these two methods is only apparent; optical principles used to decode the secret are completely different.

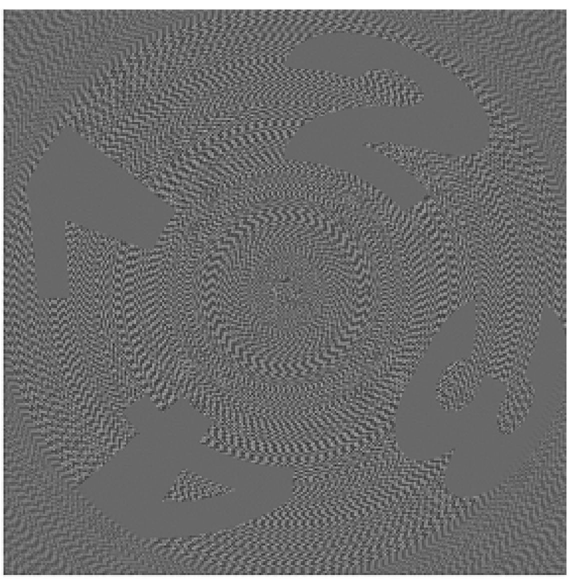

Fig. 11. Computational decryption of the secret image at a = 0.0383.

In order to improve the visibility of the decrypted text we will apply contrast enhancement procedure [20, 21] to visualize the secret information (Fig. 12).

Classical contrast enhancement techniques applicable for patterns of time-averaged moire´ fringes comprise two basic steps [20]. First, the digital image is filtered using grayscale level adjustment transformation where levels around 0.5 are mapped to 0 (middle gray levels are mapped to black color); all other grayscale levels are mapped to 1 (grayscale levels except middle gray are mapped to white color). The second step is application of morphological operations to eliminate parasitic interference lines generated by high special frequency components originating from the initial moiré grating. It can be noted that applicability of phase-stepping techniques [22] for visualization of time average moire´ fringes cannot be used directly, because grayscale level at moire´ fringe centerlines is 0.5 (not 0 as for time-averaged fringes produced by laser holography [23]).

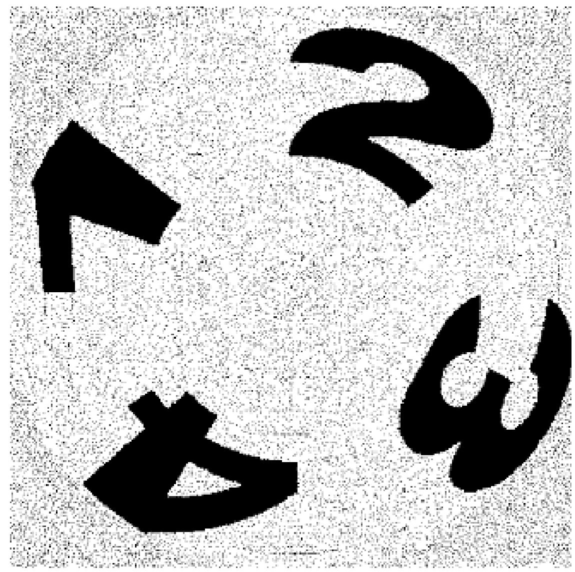

Fig. 12. Contrast enhancement of the decrypted image.

The mapping function $F(M_T(x, y))$ used for contrast enhancement must satisfy several basic requirements:

(i) $F:[0,1]\to[0,1]$;

(ii) $F(c)=0$;

(iii) $F:[c-\varepsilon, c+\varepsilon]\to[0,\delta]$ or alternatively, $F:[0,c-\varepsilon]\cup[c+\varepsilon,1]\to[1-\delta,1]$;

(iv) $F(\xi)=F(2c-\xi)$; $\xi\in[0,1]$; (13)

where ε, δ > 0; $0<c<1$. The second condition requires that the mapped grayscale color at the centreline of time-averaged fringe must be black ($c=0.5$ for time-average geometric moiré). The third condition requires that levels in a 2ε bandwidth around c are mapped to grayscale levels not higher than δ (dark color), or alternatively, the levels outside 2ε band around c are mapped to levels not lower than $1-\delta$ (bright color). The fourth requirement necessitates that the mapping function is symmetric in respect to c (ξ is the grayscale level).

Many mapping functions satisfy the up-mentioned requirements; we will mention few functions. Step mapping function:

$$F(M_T(x,y)) = \begin{cases} 0, \text{ when } c-\varepsilon \le M_T(x,y) \le c+\varepsilon \\ 1, \text{ elswhere} \end{cases} \tag{14}$$

Characteristic feature of step mapping function is that the continuous grayscale interval is mapped into pure black and white colors. This feature can be advantageous in certain applications, especially when subsequent morphological operations are used (it can be easier to manipulate with only black and white pixels). The drawback is the problematic location of the fringe centers in the mapped image. Even very small ε will not eliminate parasitic fringes from the mapped image (true fringes will be also thin then). Subsequent morphological operations can wipeout not only parasitic but also true fringes.

The pencil mapping function:

$$F(M_T(x,y)) = \begin{cases} \frac{1}{\varepsilon}\left|M_T(x,y)-c\right|, \text{ when} \\ c-\varepsilon \le M_T(x,y) \le c+\varepsilon; \\ 1, \text{ elswhere.} \end{cases} \tag{15}$$

Pencil mapping functions are advantageous when centerlines of time-averaged fringes are to be determined. The drawback is associated with problematic applicability of morphological operations for wiping out parasitic fringes. Potential of pencil functions can be fully revealed when step functions are used to enhance the time-averaged image. Initially, parasitic fringes are wiped out and then the produced pattern is used as a mask to reconstruct the original grayscale levels (only in the regions of mapped black fringes). The pencil function then can be effectively used to reconstruct fringe centerlines in the region-of-interest portions of the original image.

Square of the sigmoidal function:

$$F(M_T(x,y)) = \tanh^2(kM_T(x,y)-c). \tag{16}$$

Hyperbolic tangent and square of hyperbolic tangent are widely used in neural networks and image processing [24]. Coefficient k determines the sharpness of the mapped fringe [17]. Application of this function is advantageous in the sense that the mapped image does not have any sharp boundaries (square of hyperbolic tangent is a continuous function).

Nevertheless, the square of the sigmoidal function does not eliminate the problem of parasitic fringes. Moreover, wiping out of parasitic fringes can be even more complex compared to step functions.

The contrast enhanced decrypted image is illustrated in Fig. 12. We use square of the sigmoidal mapping function at $c=0.5$ and $\varepsilon=0.05$. It can be noted that the secret image is very well visualized in the time-averaged image. Parasitic fringes are visible in the background, but we do not use any morphological operations to eliminate them since they do not compromise the interpretation of the secret image.

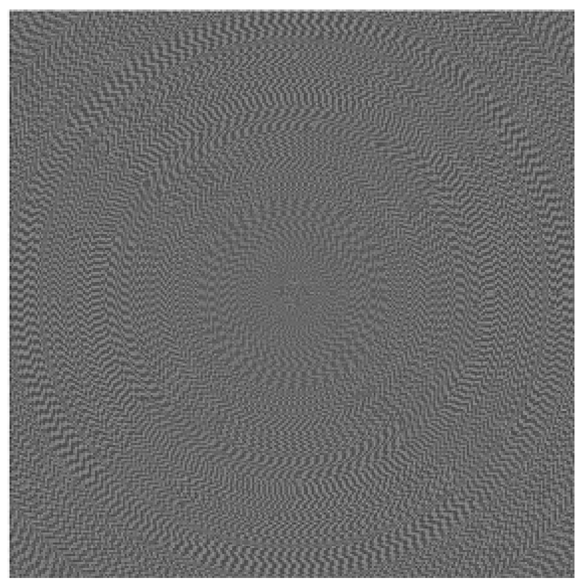

Fig. 13. Decryption is impossible when the amplitude of oscillations is not correct; a = 0.0428.

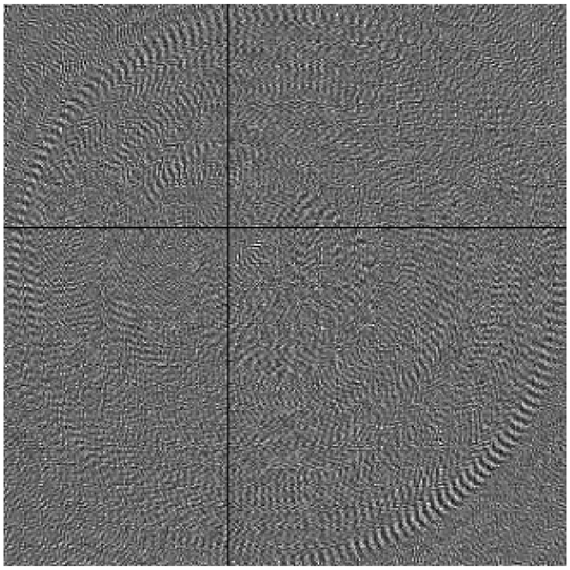

Fig. 14. Decryption is impossible when the center point of angular oscillations is not correct; a = 0.0383.

Exact selection of the central point of angular oscillations also plays an important role in the process of the image decryption. Fig. 14 illustrates that the secret image cannot be decrypted even when the amplitude of oscillations is correct (but the center of angular oscillations is wrong).

4 Conclusion

A new image hiding technique based on time-averaged moiré is presented in this paper. The encoded secret image is not shared into components; this is a one image method. The secret image is embedded into the background circular moiré grating. Stochastic initial phase deflection of circular moiré gratings help to construct an encoded digital image which cannot be interpreted by a naked eye. The decoding is performed by vibrating the encoded image in an angular direction around predefined axial point. The decoding process exploits the property of the human visual system to average fast dynamical processes being not able to follow rapid oscillatory motions.

References:

[1] M. Naor, A. Shamir, Visual Cryptography, *Lecture Notes in Computer Science*, Vol. 950, 1995, pp. 1-12.

[2] M. Ulutas, R. Yazici, V.V. Nabiyev, G. Ulutas, (2,2)-Secret Sharing Scheme with Improved Share Randomness, *23rd Int. Symposium on Computer and Information Sciences*, 2008, pp. 23-27.

[3] S.J. Shyu, Image encryption by multiple random grids, *Pattern Recognition*, Vol. 42, No. 7, 2009, pp. 1582-1596.

[4] J. Chen, T.S. Chen, H.C. Hsu, Y.H. Lin, Using multi-ringed shadow image of visual cryptography to hide more secret messages, *Journal of Imaging Science*, Vol. 57, No. 2, 2009, pp. 101-108.

[5] F. Liu, C.K. Wu, X.J. Lin, Colour visual cryptography schemes, *Information Security*, Vol. 2, No.4, 2008, pp. 151-165.

[6] R. Sirhindi, S. Murtaza, M. Afzal, Improved Data Hiding Technique for Shares in Extended Visual Secret Sharing Schemes, *Lecture Notes in Computer Science*, Vol. 5308, 2008, pp. 376-386.

[7] J.B. Feng, H.C. Wu, C.S. Tsai, Y.F. Chang, Y.P. Chu, Visual secret sharing for multiple secrets, *Pattern Recognition*, Vol. 41, No. 12, 2008, pp. 3572-3581.

[8] C.N. Yang, T.S. Chen, Colored visual cryptography scheme based on additive color mixing, *Pattern Recognition*, Vol. 41, No. 10, 2008, pp. 3114-3129.

[9] S. Cimato, R. De Prisco, A. De Santis, Colored visual cryptography without color darkening, *Theoretical Computer Science*, Vol. 374, No. 1-3, 2007, pp. 261-276.

[10] A.S. Kobayashi, *Handbook on Experimental Mechanics*, 2nd ed., Bethel, The Society for Experimental Mechanics, 1993.

[11] K. Patorski, M. Kujawinska, *Handbook of the Moiré Fringe Technique*, Elsevier, 1993.

[12] F.L. Dai, Z.Y Wang, Geometric micron moiré, *Optics and Lasers in Engineering*, Vol. 31, 1999, pp. 191-198.

[13] Y. Desmedt, T. Van Le, Moiré cryptography, *7th ACM Conf. on Computer and Communications Security*, 2000, pp. 116–24.

[14] G. Nebanon, A.M. Bruckstein, On desiging moiré patterns, *Lecture Notes in Computer Science*, Vol. 2134, 2001, pp. 185-201.

[15] M. Ragulskis, A. Aleksa, Image hiding based on time-averaging moiré. *Optics Communications*, Vol. 282, No. 14, 2009, pp. 2752-2759.

[16] M. Ragulskis, A. Aleksa, Z. Navickas, Image hiding based on time-averaged fringes produced by non-harmonic oscillations, *Journal of Optics A: Pure and Applied Optics*, Vol. 11, No. 12, 2009, Art.No. 125411.

[17] M. Ragulskis, L. Saunoriene, Applicability of optical geometric differentiation for time-average geometric moiré, *Strain*, Vol. 42, No. 3, 2006, p. 173-179.
[18] M. Ragulskis, Z. Navickas, Time average moire - back to the basics, *Experimental Mechanics*, Vol. 49, No. 8, 2009, p. 439-450.
[19] M. Ragulskis, A. Aleksa, L. Saunoriene, Improved algorithm for image encryption based on stochastic geometric moire and its application, *Optics Communications*, Vol. 273, No. 2, 2007, p. 370-378.
[20] M. Ragulskis, A. Aleksa, R. Maskeliunas, Contrast enhancement of time averaged fringes based on moving average mapping functions, *Optics and Lasers in Engineering*, Vol. 47, No. 7-8, 2009, pp. 768-773.
[21] Chanming Sun, Moving average algorithms for diamond, hexagon, and general polygonal shaped window operations, *Pattern Recognition Letters*, Vol. 27, No. 6, 2006, pp. 556-566.
[22] P.H. Chan, P.J. Bryanston-Cross, S.C. Parker, Spatial phase stepping method of fringe-pattern analysis, *Optics and Lasers in Engineering*, Vol. 23, No. 5, 1995, pp. 343-354.
[23] C.M. West, *Holographic interferometry*, New York: Wiley, 1979.
[24] R. Cancelliere, M. Gai, A comparative analysis of neural network performances in astronomical imaging, *Applied Numerical Mathematics*, Vol. 45, No. 1, 2003, pp. 87–98.